

A *Q*-switched erbium-doped fiber laser based on ZrS₂ as a saturable absorber

Ping Hu (胡平), Yan Huang (黄燕), Fangfang Liu (刘芳芳), Ying Liu (刘英), Liping Guo (郭立萍), Xiaolu Ge (葛筱璐), and Xiaojuan Liu (刘晓娟)*

School of Physics and Optoelectronic Engineering, Shandong University of Technology, Zibo 255049, China

*Corresponding author: liuxiaojiansd@163.com

Received March 22, 2019; accepted May 6, 2019; posted online July 9, 2019

A passively *Q*-switched erbium-doped fiber (EDF) laser is proposed and demonstrated utilizing a zirconium disulfide (ZrS₂)-based saturable absorber (SA). ZrS₂ nanosheets are prepared, whose modulation depth, saturation intensity, and nonsaturable absorbance are measured to be 14.7%, 0.34 MW/cm², and 17.4%, respectively. Then, a *Q*-switched EDF laser is implemented by the ZrS₂-SA. The pulse repetition rate varies from 40.65 to 87.1 kHz when the pump power changes from 55 to 345 mW. The shortest pulse width is 1.49 μs with pulse energy of 33.5 nJ. As far as we know, this is the shortest pulse width obtained by a ZrS₂-SA so far.

OCIS codes: 060.2410, 060.3510, 160.4330, 320.7090.

doi: 10.3788/COL201917.080603.

Short-pulse all-fiber lasers have been extensively investigated for widespread industry and scientific research applications such as remote sensing, industrial processing, laser medicine, fiber optic communication, and spectroscopy fields^[1-3]. The *Q*-switched mechanism is mainly involved for short-pulse generation with pulse durations of microsecond (μs) or nanosecond (ns) level and low repetition rate of kilohertz (kHz)^[4,5]. The dominant technology is based on a passively *Q*-switched scheme, which, at present, is mainly enabled by a kind of nonlinear element, i.e., a saturable absorber (SA)^[6-8].

On the other hand, in the race towards two-dimensional (2D) electronic and optoelectronic devices, semiconducting transition metal dichalcogenides (TMDCs) from group VIB have been intensively studied, while semiconducting TMDCs from group IVB have been verified to have larger mobility than their counterparts from group VIB in the monolayer. Among those, zirconium disulfide (ZrS₂) is a typical group IVB TMDC material, which has gained much research attention since 1970^[9-11]. Its electron mobility is 1200 cm²/(V · s), which is close to four times that of MoS₂ [340 cm²/(V · s)]^[12], and the current density is also higher than MoS₂. Besides, ZrS₂ shows good thermodynamic stability, environmental friendliness, high sensitivity, and low-cost production^[13-16]. So far, 2D monolayer ZrS₂ has been successfully applied in photodetectors^[17], solar cells^[18], high-electron-mobility transistors (HEMTs)^[19], and so on. However, the research on pulse lasers based on the saturable absorption characteristics of ZrS₂ has hardly been reported at home and abroad except that in 2019; for the first time, to the best of our knowledge, Li *et al.* successfully realized a dual-wavelength passively *Q*-switched operation in an erbium-doped fiber (EDF) laser using a ZrS₂-based SA^[2] deposited on a D-shaped fiber.

In this Letter, firstly, ZrS₂ nanosheets are successfully prepared and the SA characteristics are studied. The modulation depth, saturation intensity, and nonsaturable

absorbance are 14.7%, 0.34 MW/cm² and 17.4% at 1.55 μm, respectively. Secondly, a *Q*-switched EDF laser operation is achieved by ZrS₂-based SA. The pulse repetition rate varies from 40.65 to 87.1 kHz with the increasing pump power. The shortest pulse width is 1.49 μs with a single pulse energy of 33.5 nJ, which, to the best of our knowledge, is the shortest pulse width obtained by a ZrS₂-SA so far. The results show that a ZrS₂-based SA has great potential in the application in pulse fiber laser operation. Comparatively, the SA based on a D-shaped fiber displays the polarization-dependent absorption, which has been studied in Ref. [20], while the transmission-type SA in our work is insensitive to the polarization. On the other hand, although the advantage of an SA based on a D-shaped fiber is to improve the damage threshold, the SA in this work is not damaged under high pump power due to the great thermal stability. Besides, compared to other new materials enabling the *Q*-switched and mode-locked process, such as iron oxide nanoparticles (IONP), Fe₃O₄, and MoS₂/SiO₂^[21-23], ZrS₂ has advantages of larger modulation depth and lower saturation intensity, which enables a wider application scope. This work expands the applications of IVB TMDCs as SAs for pulse fiber lasers and is worthy for improving optoelectronic devices. Higher pulse energy and shorter pulse duration can be realized by further optimizing the EDF laser cavity and the ZrS₂ SA.

At the beginning of the experiment, 60 mg high lattice quality bulk ZrS₂ crystal is dispersed into 60 mL isopropyl alcohol (IPA) solvent. After 10 h ultrasonication at low temperature, the dispersion solution is further centrifuged at a rate of 6000 r/min for 30 min until the ZrS₂ is thoroughly dispersed, and the upper 80% solution is selected for the subsequent experiments. As shown in Fig. 1, the photograph of the homogeneous ZrS₂ dispersion displays a light yellow color. After that, 400 mg polyvinyl acetate (PVA) is added into 10 mL ZrS₂ dispersion, and the



Fig. 1. ZrS₂ nanosheets dispersion solution.

mixture undergoes the 1 h ultrasonication process to prepare uniform ZrS₂-PVA-IPA dispersion. PVA is used as the polymer matrix, not only to form film to host the ZrS₂, but also to avoid its oxidation. A single drop of the obtained ZrS₂ solution is immersed on the end of the fiber. Then, the sample is dried for 24 h at a temperature of 25°C, and, finally, the ZrS₂ SA is obtained.

A transmission electron microscopy (TEM) image is taken and shown in Fig. 2. It is seen that the ZrS₂ nanosheets exhibit an obvious layered structure. The radial size of the ZrS₂ nanosheets is about 120 nm. The Raman spectrum of the processed ZrS₂ nanosheets is tested with an Ar laser operating at the wavelength of 514 nm, and the result is shown in Fig. 3. The in-plane mode (E_g) and out-of-plane mode (A_{1g}) can be clearly observed in Fig. 3. The A_{1g} peak is located at 332.24 cm⁻¹, while the E_g peak is at 250.12 cm⁻¹. Due to the non-harmonic effect, the peak at the “*” is widened, which is consistent with the existing research reports^[11].

The nonlinear optical absorption properties of the ZrS₂-based SA are investigated by the commonly used balanced twin-detector measurement scheme, where a fiber laser operating at central wavelength of 1550 nm with 6 ns pulse duration and fundamental frequency of 10 Hz is utilized. The nonlinear power-dependent normalized saturable absorption curve of the ZrS₂-based SA is shown as blue dots in Fig. 4. As the light intensity gradually increases, the nonlinear optical transmission

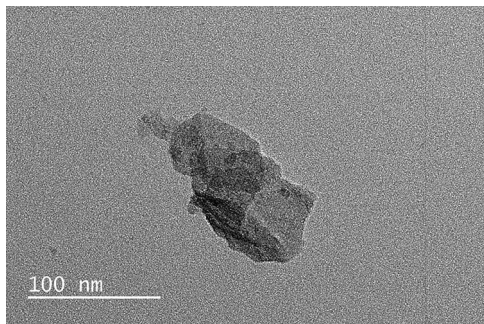


Fig. 2. TEM image of the ZrS₂ nanosheets.

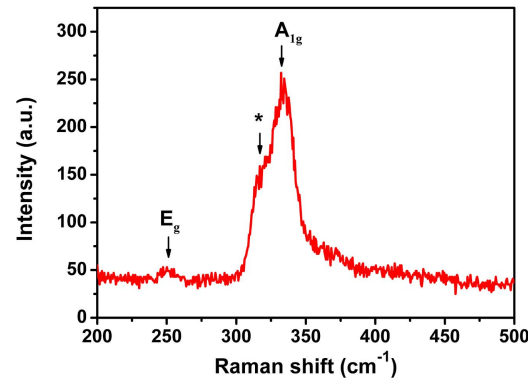


Fig. 3. Raman spectrum of the ZrS₂ nanosheets.

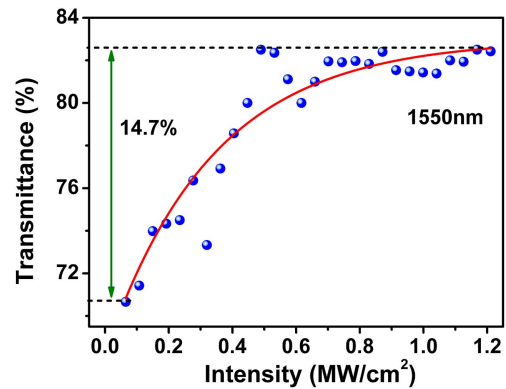


Fig. 4. Saturable absorption property of ZrS₂-PVA film.

approximately increases to 83% and remains saturated, which exhibits a typical saturable absorption characteristic. The modulation depth, saturation intensity, and non-saturable absorbance are 14.7%, 0.34 MW/cm², and 17.4%, respectively. The red line in Fig. 4 displays the curve of the saturable absorption formula:

$$T = 1 - \frac{\alpha_s}{1 + \frac{I}{I_{\text{sat}}}} - \alpha_{\text{ns}}, \quad (1)$$

where T is transmission, I is input source intensity, I_{sat} is saturation intensity, and α_s and α_{ns} are the modulation depth and nonsaturable absorbance, respectively. It is seen that the data matches closely to the formula.

The schematic of the passively Q -switched EDF laser using the ZrS₂-based SA is given in Fig. 5, where the laser cavity shows the ring-shaped structure. A commercial 976 nm laser diode with a maximum power of 400 mW is used as a pump, which is coupled into the laser cavity through 980/1550 wavelength-division multiplexing (WDM). A 6-m-long EDF (LIEKKI: Er110-4-125) is used as the gain medium. The prepared ZrS₂-based SA is inserted into the cavity after the EDF. A polarization-independent isolator (PI-ISO) is used to ensure the unidirectional operation of laser cavity. A polarization controller (PC) is used to optimize the cavity birefringence. Additionally, 20% of the laser power is extracted

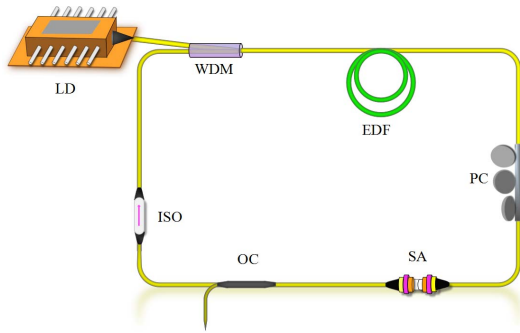


Fig. 5. Experimental setup of Q -switched EDF laser.

from the cavity using an optical coupler (OC). The length of the cavity, including the EDF and the tail fibers, is about 11 m. The output spectrum, the pulse trace, and the average output power are detected by a spectrum analyzer (YOKOGAWA AQ6370B), a digital oscilloscope (Tektronix DP04104), and a power meter (Moletron PM3), respectively.

The system operates in a stable Q -switched state in the 55–345 mW pump range, and the pulse trains versus different pump powers are shown in Fig. 6. The Q -switched pulse sequence remains highly stable during the whole experiment period, even the prepared ZrS_2 SA is exposed into the air, which reveals the fact that the ZrS_2 -PVA mixture film protects ZrS_2 from oxidation in air.

The variation of the repetition rate and pulse width along with the increasing pump power is shown in Fig. 7(a). When the pump power is increasing from 55 to 345 mW, the Q -switched pulse width decreases from 9.28 to 1.49 μ s, while the repetition rate increases from 40.65 to 87.1 kHz, which is the typical characteristic of passively Q -switched lasers. The shortest pulse width of 1.49 μ s is obtained when the pump power is up to 345 mW with a repetition rate of 86.2 kHz. Besides, a single pulse shape is recorded at the same time, which is shown in Fig. 7(b), while the insert shows a typical Q -switched pulse sequence with a repetition rate of 40.65 kHz. The pulse sequence is stable, and there is no significant jitter on the oscilloscope. In Ref. [9], the interaction between the laser and ZrS_2 materials is much

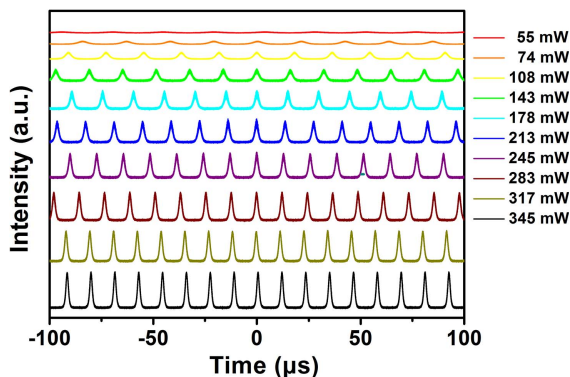


Fig. 6. Pulse trains at different pump powers.

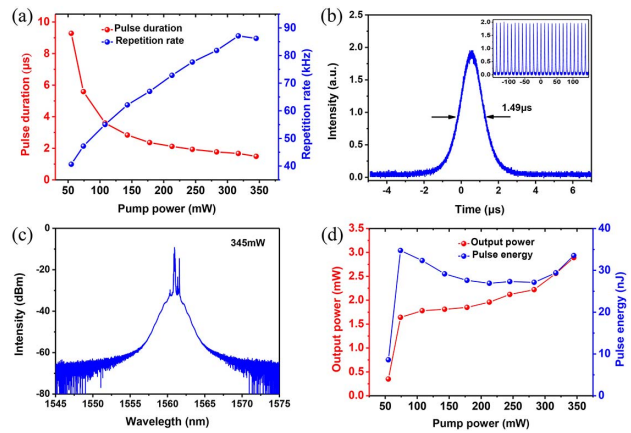


Fig. 7. (a) The pulse duration and pulse repetition rate versus the pump power. (b) The typical single pulse sharp of the Q -switched fiber laser. The inset is the output pulse train. (c) The output spectrum of the Q -switched fiber laser. (d) The output power and pulse energy versus the pump power.

longer, which is helpful for shortening the Q -switched pulse duration. However, the modulation depth of the ZrS_2 SA is rather low while the saturable intensity is high, which is not suitable to generate a short pulse. Comparatively, the ZrS_2 SA in our work has larger modulation depth and lower saturation intensity. This combination might explain why the pulse duration is shortened, although the interaction length is relatively much shorter.

Figure 7(c) shows the output spectrum of the system. It reveals a center wavelength of 1560.91 nm with a 3 dB linewidth of 1.5 nm. Figure 7(d) depicts that when the pump power is increased, the output power and the single pulse energy increase simultaneously. When the pump power is 345 mW, the maximum average output power of 2.89 mW is obtained with energy of 33.5 nJ for each pulse, corresponding to optical-to-optical efficiency and slope efficiency of 0.84% and 0.88%, respectively. Limited to the available pump power in our lab, the pump power limit of the ZrS_2 -based SA cannot be tested. It is believed that the pulse energy can be further improved by several means, such as increasing the pump power, optimizing the splitting ratio of the OC, and optimizing the ZrS_2 SA parameters and cavity design. Such measures have been also discussed in Ref. [5]. From the obtained results, the prepared ZrS_2 SA presents great thermal stability and is qualified for higher pump power.

The repetition rate and the pulse energy show decreasing trends at pump powers of 317 and 78 mW, respectively. Similar results can be observed in many previous reports [5,21,24,25]. The generally accepted reason is that, when the pump power is high enough, the nonlinear effect in the fiber increases due to the high light intensity, which leads to the instability of the pulse energy and pulse repetition rate. Specific to our work, some imperfection of the ZrS_2 SA combined with other factors such as saturable recovery time, saturable threshold of the SA, and the gain saturation of the EDF might also affect the evolution of

the pulses in the cavity. Although we cannot implement the verifying experiment at present due to the limited pump power, it can be predicted that the repetition rate will increase again along with the increasing pump power because the results presented in Fig. 7(d) show no thermal damage on the ZrS₂ SA or ultra-saturation of the ZrS₂ SA.

For comparison, we summarize the performance of different SA-based *Q*-switched EDF lasers implemented around 1550 nm and presented in Table 1. The experimental results achieved in our work indicate that ZrS₂ SA can perform excellently in the *Q*-switched process. Higher pulse energy and shorter pulse duration can be realized by further optimizing the EDF laser cavity and the ZrS₂ SA.

Can the ZrS₂ SA be used for mode-locked operation? According to the criterion of mode-locked operation^[32], $E_P^2 > E_G E_{SA} \Delta T$, where E_P is the single pulse energy in the cavity, and E_G and E_{SA} are the saturation energy of the gain fiber and the SA, respectively. ΔT is the modulation depth of the SA. It is seen that decreasing the modulation depth of the SA will benefit mode-locked generation. However, in our work, the ZrS₂ SA has a higher modulation depth, which is one of the reasons why there are no mode-locked pulses during the experiment. It can be surmised that the mode-locked fiber laser will be realized by a ZrS₂ SA with suitable parameters, including the layer number of ZrS₂ and ZrS₂ concentration in the ZrS₂-PVA dispersion. Additionally, the length of the EDF and the total length of the cavity are 6 and 11 m, respectively. The long gain medium of the EDF and the quite short cavity are not suitable to achieve mode-locked pulses. In the following experiment, in order to achieve mode-locked pulses, we plan to do such works as the following: utilizing a shorter EDF, lengthening the cavity, optimizing the ZrS₂ SA parameters, such as reducing the modulation depth of the ZrS₂ SA, as well as optimizing the cavity, such as decreasing the inner loss of the

Table 1. Comparison of Passively *Q*-switched Er-doped Fiber Lasers Based on Different SAs

SA	Wavelength (nm)	Pulse Width (μs)	Pulse Energy (nJ)	Max Output Power (mW)	Refs.
Graphene	1556.17	3.7	16.7	1.1	[26]
SWNTs	1555–1560	7	14.1	0.225	[27]
MoS ₂	1519–1567	3.3	160	5.91	[28]
InSe	1532.2	8.3	112.97	1.425	[25]
BP	1562.87	10.32	94.3	1.5	[29]
Bi ₂ Se ₃	1565	1.9	23.7	22.35	[30]
NiO	1522–1580	2.02	15.3	2.32	[31]
ZrS ₂	1560.91	1.49	33.5	2.89	Our work

cavity. Additionally, we will make an effort to match the optimized cavity well with the ZrS₂ SA.

In order to verify the effect of the ZrS₂-based SA on the EDF laser, we remove the SA and keep the cavity length unchanged. The *Q*-switched pulse vanishes no matter how the PC and the pump power are adjusted. The comparison proves that ZrS₂ is an excellent SA and can implement *Q*-switched fiber lasers efficiently.

In summary, a ZrS₂-based SA is successfully prepared, and its characteristics are studied. The modulation depth, saturation intensity, and nonsaturable absorbance of ZrS₂ SA are measured to be 14.7%, 0.34 MW/cm², and 17.4%, respectively. Then, the prepared ZrS₂ SA is inserted into a ring EDF laser cavity to implement the *Q*-switched operation successfully. The pulse repetition rate changes from 40.65 to 87.1 kHz when the pump power increases from 55 to 345 mW. The shortest pulse width is 1.49 μs, the maximum output power is 2.89 mW, and the maximum single pulse energy is 33.5 nJ, respectively. The experimental results verify that the layered structure ZrS₂ can be used as a highly efficient SA for fiber lasers. This work expands the applications of IVB TMDCs as SAs for pulse fiber lasers and has great significance for the development of optoelectronic devices.

The work was supported by the National Natural Science Foundation of China (No. 11304184) and partially supported by the National Natural Science Foundation of China (No. 11704226) and the Natural Science Foundation of Shandong Province (No. ZR2017MA051). We acknowledge Yudong Cui from Zhejiang University for the full discussions with him.

References

1. M. Laroche, A. M. Chardon, J. Nilsson, D. P. Shepherd, W. A. Clarkson, S. Girard, and R. Moncorge, *Opt. Lett.* **27**, 1980 (2002).
2. D. J. Richardson, J. Nilsson, and W. A. Clarkson, *J. Opt. Soc. Am. B* **27**, B63 (2010).
3. H. Ahmad, F. D. Muhammad, C. H. Pua, and K. Thambiratnam, *IEEE J. Sel. Top. Quantum Electron.* **20**, 166 (2014).
4. H. Ahmad and S. A. Reduan, *Chin. Opt. Lett.* **16**, 010609 (2018).
5. R. Z. R. Rosdin, F. Ahmad, N. M. Ali, S. W. Harun, and H. Arof, *Chin. Opt. Lett.* **12**, 091404 (2014).
6. X. Dong, J. Tian, Z. Yu, and Y. Song, *Chin. Opt. Lett.* **12**, S21402 (2014).
7. H. Ahmad, S. N. Aidit, S. I. Ooi, and Z. C. Tiu, *Chin. Opt. Lett.* **16**, 020014 (2018).
8. M. Liu, W. Liu, P. Yan, S. Fang, H. Teng, and Z. Wei, *Chin. Opt. Lett.* **16**, 020007 (2018).
9. L. Li, R. Lv, J. Wang, Z. Chen, H. Wang, S. Liu, W. Ren, W. Liu, and Y. Wang, *Nanomaterials* **9**, 315 (2019).
10. X. Wang, L. Huang, X. Jiang, Y. Li, Z. Wei, and J. Li, *J. Mat. Chem. C* **4**, 3143 (2016).
11. S. Mañas-Valero, V. García-López, A. Cantarero, and M. Galbiati, *Appl. Sci.* **6**, 264 (2016).
12. T. Kanazawa, T. Amemiya, A. Ishikawa, V. Upadhyaya, K. Tsuruta, T. Tanaka, and Y. Miyamoto, *Sci. Rep.* **6**, 22277 (2016).
13. W. Zhang, Z. Huang, W. Zhang, and Y. Li, *Nano Res.* **7**, 1731 (2014).

14. M. Zhang, Y. Zhu, X. Wang, Q. Feng, S. Qiao, W. Wen, Y. Chen, M. Cui, J. Zhang, C. Cai, and L. Xie, *J. Am. Chem. Soc.* **137**, 7051 (2015).
15. H. Jiang, *J. Chem. Phys.* **134**, 204705 (2011).
16. C. Gong, H. Zhang, W. Wang, L. Colombo, M. W. Robert, and C. Kyeongjae, *Appl. Phys. Lett.* **103**, 329 (2013).
17. L. Li, X. Fang, T. Zhai, M. Liao, U. K. Gautam, X. Wu, Y. Koide, Y. Bando, and D. Golberg, *Adv. Mater.* **22**, 4151 (2010).
18. L. Li, H. Wang, X. Fang, T. Zhai, Y. Bando, and D. Golberg, *Energy Environ. Sci.* **4**, 2586 (2011).
19. Q. Wang, K. Kalantar-Zadeh, A. Kis, J. N. Coleman, and M. S. Strano, *Nat. Nanotechnol.* **7**, 699 (2012).
20. Y. Cui, F. Lu, and X. Liu, *Sci. Rep.* **7**, 40080 (2017).
21. L. Pang, C. Song, R. Lv, Z. Chen, S. Liu, R. Wu, Y. Lv, and W. Liu, *Opt. Laser Technol.* **113**, 379 (2019).
22. L. Li, R. Lv, S. Liu, Z. Chen, J. Wang, Y. Wang, W. Ren, and W. Liu, *Opt. Mater. Express* **9**, 731 (2019).
23. L. Li, R. Lv, Z. Chen, J. Wang, S. Liu, W. Ren, and Y. Wang, *Nano-scale Res. Lett.* **14**, 59 (2019).
24. J. Wang, Y. Xing, L. Chen, S. Li, H. Jia, J. Zhu, and Z. Wei, *J. Lightwave Technol.* **36**, 2010 (2018).
25. W. Yang, N. Xu, and H. Zhang, *Laser Phys. Lett.* **15**, 105101 (2018).
26. Z. Luo, M. Zhou, J. Weng, G. Huang, H. Xu, C. Ye, and Z. Cai, *Opt. Lett.* **35**, 3709 (2010).
27. D. Zhou, L. Wei, B. Dong, and W. Liu, *IEEE Photon. Technol. Lett.* **22**, 9 (2010).
28. Y. Huang, Z. Luo, Y. Li, M. Zhong, B. Xu, K. Che, H. Xu, Z. Cai, J. Peng, and J. Weng, *Opt. Express* **22**, 25258 (2014).
29. Y. Chen, G. Jiang, S. Chen, Z. Guo, X. Yu, C. Zhao, H. Zhang, Q. Bao, S. Wen, D. Tang, and D. Fan, *Opt. Express* **23**, 12823 (2015).
30. Z. Yu, Y. Song, J. Tian, Z. Dou, H. Guoyu, K. Li, H. Li, and X. Zhang, *Opt. Express* **22**, 11508 (2014).
31. H. Ahmad, S. A. Reduan, and N. Yusoff, *RSC Adv.* **8**, 25592 (2018).
32. U. Keller, *Nature* **424**, 831 (2003).